

Multifunctional Nanoparticles by Coordinative Self-Assembly of His-Tagged Units with Metal–Organic Frameworks

Ruth Röder,[†] Tobias Preiß,[‡] Patrick Hirschle,[§] Benjamin Steinborn,[†] Andreas Zimpel,[§] Miriam Höhn,[†] Joachim O. Rädler,[‡] Thomas Bein,[§] Ernst Wagner,[†] Stefan Wuttke,^{*,§} and Ulrich Lächelt^{*,†}

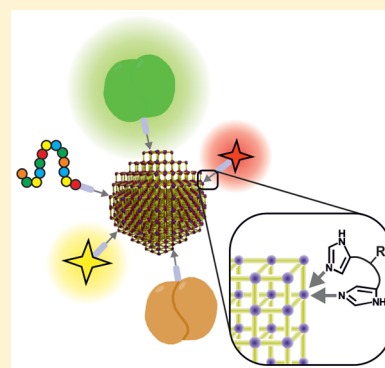
[†]Pharmaceutical Biotechnology, Department of Pharmacy and Center for NanoScience (CeNS), LMU Munich, 81377 Munich, Germany

[‡]Department of Physics and Center for NanoScience (CeNS), LMU Munich, 80539 Munich, Germany

[§]Department of Chemistry and Center for NanoScience (CeNS), LMU Munich, 81377 Munich, Germany

Supporting Information

ABSTRACT: Self-assembly of individual units into multicomponent complexes is a powerful approach for the generation of functional superstructures. We present the coordinative interaction of oligohistidine-tags (His-tags) with metal–organic framework nanoparticles (MOF NPs). By this novel concept, different molecular units can be anchored on the outer surface of MOF NPs in a self-assembly process generating multifunctional nanosystems. The article focuses on two main objectives: first, the detailed investigation of the assembly process and fundamental establishment of the novel functionalization concept; and second, its subsequent use for the development of biomacromolecule (e.g., peptides and proteins) delivery vehicles. Three exemplary MOF structures, MIL-88A, HKUST-1, and *Zr-fum*, based on different metal components, were selected for the external binding of various His-tagged synthetic peptides and recombinant or chemically H₆-modified proteins. Evidence for simultaneous assembly of different functional units with *Zr-fum* MOF NPs as well as their successful transport into living cells illustrate the promising potential of the self-assembly approach for the generation of multifunctional NPs and future biological applications. Taking the high number of possible MOF NPs and different functional units into account, the reported functionalization approach opens great flexibility for the targeted synthesis of multifunctional NPs for specific purposes.



INTRODUCTION

Nanoparticles (NPs) that combine different functional domains are of high interest for various scientific disciplines requiring multifunctionality at the nanoscale. The controlled manipulation of the external surface of NPs is of paramount importance as it defines the interface between the NP and its surroundings and strongly determines the overall performance of the NP especially in biological environments.^{1,2} Researchers have shown that surface functionalization is a powerful tool for the creation of programmable NP interfaces. In this respect, the self-assembly of the functional units onto the NPs surface appears as a powerful approach because it would ensure a defined arrangement of these units without any guidance from an external source. Examples of self-assembly processes used for the generation of multifunctional colloidal NPs are micelle, liposome, or polymeric formation of amphiphilic compounds^{3–6} and cyclodextrin-adamantane host–guest interactions.^{7,8} Especially for biomedical applications, multifunctional NPs that interact with biological systems at the molecular level and perform tasks within cellular systems are in great demand.^{9,10} The intracellular delivery of biomacromolecules, such as peptides and proteins, represents a particularly challenging task. Several different barriers have to be overcome,

including cellular uptake, endosomal escape, intracellular trafficking and cargo release.^{11,12} The heterogeneity of this compound class (hydrophilicity, charge, functional groups) hampers the development of universal delivery platforms. For this reason, nanocarriers with a functionalization mode, which is independent from the individual properties of the functional units, would be advantageous.

Here, we present the coordinative interaction of oligohistidine-tags with metal–organic frameworks (MOFs) as a novel external functionalization concept for MOF NPs based on a self-assembly process. MOFs are a class of materials synthesized of inorganic building units, metal ions, or metal oxide clusters, which are coordinatively connected by organic linkers to create porous three-dimensional frameworks (Figure 1a).¹³ Their crystallinity, chemically functionalizable pores, and potential systematic structural variation are some factors among others that allow one to precisely design these materials for particular purposes.^{14,15} Regarding biomedical applications, the hybrid MOF nature provides the advantageous potential of degradability and disintegration into the low molecular weight

Received: November 18, 2016

Published: January 11, 2017

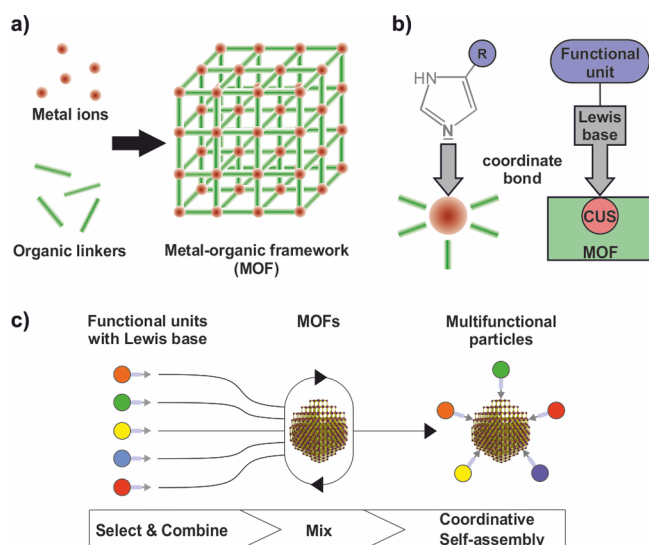


Figure 1. Illustration of coordinative self-assembly of His-tagged molecules with MOF NPs: (a) molecular composition of MOFs; (b) coordinative bond between the imidazole group of histidines acting as Lewis base and coordinatively unsaturated metal sites (CUS) acting as Lewis acid; (c) multifunctional MOF NPs generated by coordinative attachment of different functional units via self-assembly.

components which can be eliminated from the body.^{16–19} Different research groups have already reported pioneering examples of MOF NPs as transport vehicles for the delivery of biologically active molecules.^{16,20–27} Here the combination of the high MOF surface area for high drug loading and the possibility to engineer the internal surface to control MOF scaffold-guest interaction was used to optimize the nanocarrier performance.²⁸ Even biomacromolecules such as proteins, DNA or enzymes could be encapsulated into MOFs recently,^{29,30} or the MOF scaffold itself could be used as a part of the therapeutic principle.^{31–34} Therefore, combining the rich and versatile bulk chemistry of MOF materials with controlled and programmable NP interfaces may lead to novel multifunctional nanosystems.^{35–40} Our concept uses the interaction between Lewis bases, such as the imidazole function of histidine and coordinatively unsaturated metal sites (CUS) present on the external surface of MOF NPs (Figure 1b) to self-assemble different functional units (Figure 1c).

The exemplary set of (oligo)histidine-tag functional units used in this study is summarized in Table 1. Since His-tags can be readily integrated into peptides or proteins by synthetic,

recombinant or bioconjugation techniques, they appear to be ideal connectors to create a versatile inorganic/bioorganic interface at the MOF NPs' surface. The same interaction (Figure 1b) is routinely used for the purification of recombinant proteins by immobilized metal ion chromatography.^{41,42} Applicability of the coordinative His-tag interactions for intracellular delivery of proteins has been demonstrated before by using conjugates of nitrilotriacetic acid derivatives and cell-penetrating peptides,^{43,44} polymers⁴⁵ or silica NPs.⁴⁶ In these approaches, the delivery platforms and vehicles were synthetically modified with separate metal-chelators. Since the metal-sites already are an integral part of the coordinative MOF structure, the external secondary modification via coordinative bonds in the presented approach of 'self-assembling multifunctional coordination particles' (SAMCOPs) is considered a powerful tool for the combinatorial and stoichiometric generation of functional MOFs.

RESULTS AND DISCUSSION

Selection and Characterization of MOF NPs. A set of three exemplary MOF structures, MIL-88A (Fe³⁺/fumaryl acid),¹⁶ HKUST-1 (Cu²⁺/trimesic acid)⁴⁷ and Zr-*fum* (Zr⁴⁺/fumaryl acid)^{48,49} was selected for testing the assembly strategy. HKUST-1 was chosen based on the high His-tag affinity toward chelated Cu²⁺, which even exceeds affinity toward Ni²⁺ and Co²⁺.^{50,51} MIL-88A and Zr-*fum* represent well established MOFs with potential for biomedical applications.^{16,18} Although Ni²⁺, Co²⁺, and Zn²⁺ are known to have high affinity to His-tags,^{50,51} they were not included in the study due to the expected cytotoxicity of Ni²⁺ and Co²⁺ MOFs and the low stability of Zn-based MOFs in aqueous media. Together, the set covers a range of well-established MOF species with individual material characteristics and each based on a different di-, tri-, or tetravalent metal component with expected different His-tag binding capacities.

The quality of the MOF NPs used in this study was ensured by applying multiple complementary characterization techniques: scanning electron microscopy (SEM, Figures S10–S15), dynamic light scattering (DLS, Figures S1 and S2, Table S2), X-ray diffraction (XRD, Figures S3–S5), thermogravimetric analysis (TGA, Figures S6–S8), and nitrogen sorption measurements providing the surface area (Figure S9, Table S3). Powder XRD patterns were determined for all MOF NP species (Figures S3–S5). The diffractograms were used to verify the successful synthesis of the MOF species as well as to show the high crystallinity of the Zr-*fum* and HKUST-1 NPs. It

Table 1. His-tagged functional units used for the assembly with MOF NPs

code	sequence ^a /description	function
H ₆ -Acr	acridine-PEG ₂₈ -H ₆ -NH ₂	photometric detection
H _{0/3/6} -Acr	acridine-STOTDA-H _{0/3/6}	
H _{0/3/6} -FITC	FITC-STOTDA-H ₆	fluorescence detection
H ₆ -A647N	ATTO647N-PEG ₁₂ -H ₆ -NH ₂	
H ₆ -CF	carboxyfluorescein-PEG ₁₂ -H ₆ -NH ₂	
H ₆ -GFP	recombinant eGFP (H ₆ -tag)	model proteins
H ₆ -Tf*	transferrin conjugated with H ₆ -PEG ₃₆ and ATTO 647N	
H ₆ -Bak	H ₆ -GGQVGRQLAIIGDDINR-NH ₂	pro-apoptotic peptides
H ₆ -Bad	H ₆ -GNLWAAQRYGRELRRMSDEFVD-NH ₂	
H ₆ -KLK	H ₆ -GGKLAKLAKKLAKLAK-NH ₂	
H ₆ -CytC	cytochrome <i>c</i> conjugated with H ₆	pro-apoptotic protein

^aPeptide sequences are indicated from N- to C-terminus using the one-letter code for α -amino acids (H_{*n*}, *n* = number of histidines).

should be noted that the poor crystallinity of the MIL-88A NPs are expected and have been frequently reported and discussed in the literature.^{16,52–55} At the same time, XRD was used to prove the stability of the three MOFs under the later used conditions (Figures S3–S5). For additional bulk characterization, all NP species were examined with both nitrogen sorption experiments (Figure S9, Table S3) and TGA (Figures S6–S8). The microporosity of all three NP species ranging from 0.6 up to 1.5 nm was confirmed and the BET surface area yielded typical results.^{16,47–49} Thus, we have successfully synthesized the MIL-88A, HKUST-1, and *Zr-fum* MOF structures with their expected bulk properties.

In order to characterize their corresponding NP properties a combination of two techniques was used: particle size distributions were determined via scanning electron microscopy (SEM, Figures S10–S15) for the dried species and, more importantly, for the dispersed species via dynamic light scattering (DLS, Figures S1 and S2, Table S2). For *Zr-fum*, SEM measurements resulted in a diameter of (84 ± 7) nm for the dried particles. The corresponding *z*-average diameter measured via DLS in water was determined at (182 ± 4) nm with a polydispersity index (PDI) of 0.205. This deviation toward larger diameters is to some extent expected, since DLS provides the hydrodynamic diameter of the particles and is influenced among others by particle–solvent interactions and aggregation.^{56,57} The other MOFs behave similarly: DLS experiments resulted in an average intensity based diameter of (191 ± 1) nm (PDI = 0.130) for MIL-88A and (530 ± 27) nm (PDI = 0.290) for HKUST-1 with the corresponding dried particle size distributions of (61 ± 7) nm for MIL-88A and for HKUST-1 (177 ± 39) nm. We suppose that the main reason for the larger NP diameters determined using DLS is due to the fact that the MOF samples reveal agglomeration behavior in solution.⁵⁶

Photometrical Analysis of His-Tag Binding to MOF NPs. The binding of different His-tag model peptides (e.g., H_n -Acr, H_n -FITC, H_6 -A647N) to MIL-88A, HKUST-1 and *Zr-fum* in HEPES buffered glucose (HBG) at pH 7.4 was determined by the detection of residual free peptide in the supernatant after incubation and centrifugation of the MOF suspensions (Figures 2a,b,d, 3, S17, and S19, Scheme S1). An exemplary movie demonstrating the binding of H_6 -A647N to HKUST-1 MOF NPs visualized by decoloration of the supernatant after centrifugation is provided in the Supporting Information. The exclusive reduction of H_6 -Acr (in contrast to A_6 -Acr) in the supernatant, illustrated by the discrete diminution of the H_6 -Acr peak in the RP-HPLC chromatograms, represents qualitative evidence for the histidine-dependent interaction with all three investigated MOF species (Figure 2b). The peptide-specific binding was also verified by zeta potential measurements (Figure 2c) showing a significant shift toward neutrality caused by the His-tag containing derivatives only. Quantitative determination of binding as a function of histidine residues, i.e., number of Lewis base units (H_0 , H_3 , H_6) was carried out by photometric quantification of residual free peptide using a UV-photometer (Figure 2d). The amount of bound H_3 - and H_6 -peptides increased with increasing amounts of MOFs, but binding of the H_0 derivative, corresponding to no histidine residue, was generally negligible. Notably, in case of all three MOFs significantly higher peptide binding was observed with higher number of histidines (H_0 vs H_3 and H_3 vs H_6).

This correlation was additionally confirmed for *Zr-fum* via fluorescence spectroscopy by using FITC labeled peptides

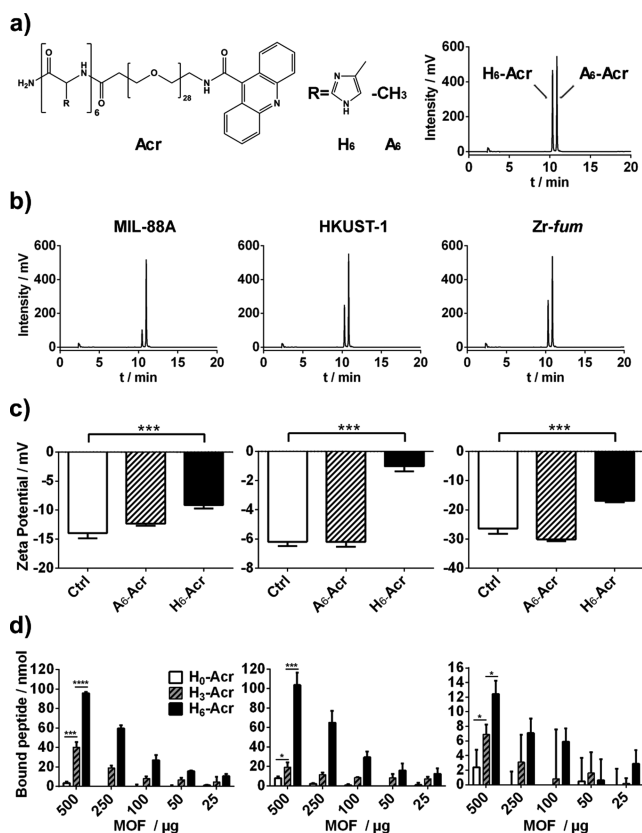


Figure 2. Acridine (Acr) peptide binding to MIL-88A (left), HKUST-1 (middle), and *Zr-fum* (right) particles in HEPES buffered glucose (HBG) at pH 7.4. (a) Chemical structure and control chromatogram of model compounds H_6 -Acr, A_6 -Acr. (b) Peptide binding (H_6 vs A_6) by detection of reduced free peptides in the supernatant (RP-HPLC, $\lambda = 360$ nm). (c) Effect of peptide binding on zeta potential. (d) Quantitative determination of bound peptides H_0 (white), H_3 (pattern), and H_6 (black) as difference to photometrically quantified free peptides in the supernatant ($\lambda = 360$ nm) using a UV-photometer. Please note that the scaling of y-axes is adjusted to the different binding capacities: 0–120 nmol peptide in case of MIL-88A and HKUST-1, 0–16 nmol peptide in case of *Zr-fum*.

($H_{0/3/6}$ -FITC) (Figure S19). Excessive addition of imidazole decreased binding of H_6 -FITC to levels of H_0 -FITC, suggesting competition of histidine and free imidazole for coordinative interaction with the MOF surface, similar to the elution of His-tagged proteins from a nickel-column in immobilized-metal ion chromatography purifications. Comparing H_6 -tag binding to 500 μ g MOF NPs, HKUST-1 achieved the highest binding (104 nmol), followed by MIL-88A (96 nmol) and *Zr-fum* (12 nmol) which is consistent with reported relative metal ion affinities ($Cu^{2+} > Fe^{3+}, Zr^{4+}$) for His-tags.⁴¹ A time course experiment (Figure 3b) revealed stable association of *Zr-fum*/ H_6 -A647N for 24 h at pH 7.4 and rapid partial (pH 5) or complete (pH 3) release upon acidification. This is consistent with the hypothesis of unprotonated histidines acting as Lewis base and being responsible for binding (Figure 3a). We suggest that the incomplete detachment at pH 5 is caused by a lowered pK_a of the imidazole group due to metal ion binding⁵⁸ and an equilibrium between protons and metal ions competing for histidine interactions.

Fluorescence Correlation Spectroscopy (FCS). Using FCS the binding of fluorescently labeled H_6 -tags to MOF particles was measured at low concentrations with single-

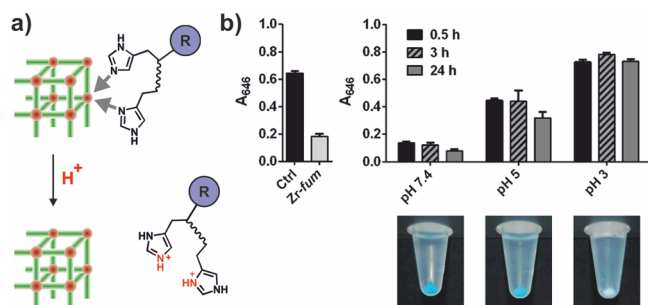


Figure 3. pH dependent stability of H₆-tag binding to Zr-fum NPs. (a) Schematic illustration of acidic detachment due to histidine protonation. (b) Experimental data obtained by photometric determination ($\lambda = 646$ nm) of free H₆-A647N in the supernatant after centrifugation. Left: Zr-fum NPs were loaded with H₆-A647N at pH 7.4 for 15 min, centrifuged and the supernatant was analyzed; Ctrl illustrates absorbance of free peptide in a sample without MOF NPs. Right: MOF NP suspensions were acidified to a defined pH and incubated for indicated times before centrifugation and analysis of the supernatant. Reaction tubes below show the MOF pellets of the same samples after 24 h at pH 7.4 (left), pH 5 (middle), and pH 3 (right) and centrifugation; decoloration of the pellet due to acidic H₆-A647N detachment at pH 3 can be observed.

molecule sensitivity (Figures 4 and S18). Figure 4 (upper left) and Figure S18 show a significant increase in the

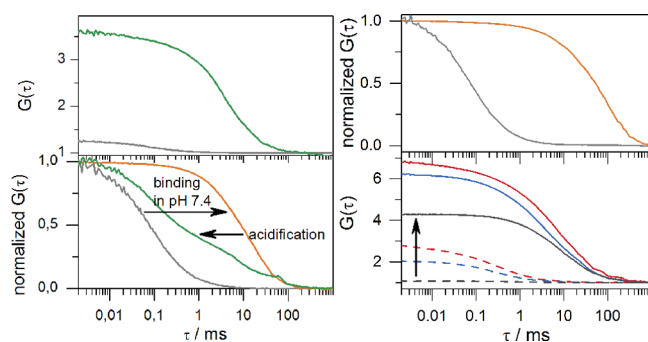


Figure 4. Investigation of Zr-fum/H₆-A647N interaction by fluorescence correlation spectroscopy (FCS). Upper left: FCS time correlation functions of H₆-A647N before (gray) and after Zr-fum NP addition (green). Lower left: Normalized time correlation functions showing binding of H₆-A647N at pH 7.4 (orange) and release upon acidification (green); free H₆-A647N (gray). Upper right: Normalized time correlation functions of measurements in DMEM (10% FBS) of free H₆-A647N (gray) and Zr-fum/H₆-A647N (orange). Lower right: fluorescence cross correlation spectroscopy (FCCS) measurements of H₆-GFP (blue) and H₆-Tf* (red) in HBG pH 7.4 before (dotted) and after (solid) Zr-fum addition. Cross correlation before (dotted gray) and after (solid gray) Zr-fum addition.

autocorrelation amplitude after addition of all three MOF species, indicating a reduction of the H₆-tag number concentration most likely due to multiple binding to MOF NPs. In case of MIL-88A and HKUST-1 (Figure S18), however, no change in the characteristic correlation decay time could be detected. We attribute this to the known phenomenon of MOF induced fluorescence quenching^{59,60} as well as rather large effective particle sizes, in particular of HKUST-1, resulting from aggregation, which both can cause a decline of detectable tags after binding. For Zr-fum NPs several key observations could be made (Figure 4). Free H₆-tags (gray) showed fast single molecule diffusion prior to NP addition

(Figure 4, lower left). After addition of Zr-fum NPs at pH 7.4 (orange) the collective diffusion was shifted toward higher diffusion times revealing H₆-tag binding to Zr-fum NPs. Following acidification (green) the diffusion rate increased relative to the pH 7.4 measurement indicating partial detachment of His-tags from the MOF NP surface, due to the protonation of histidines.

Importantly, H₆-tag association with Zr-fum NPs remained stable after dilution in DMEM medium containing 10% fetal bovine serum (FBS), confirming the suitability for use under cell culture conditions (Figure 4, upper right). Finally, two His-tagged proteins with distinct fluorescence spectra (recombinant eGFP with genetically encoded His-tag: H₆-GFP, and human transferrin chemically conjugated with a H₆-tag and ATTO 647N label: H₆-Tf*) were used for fluorescence cross correlation spectroscopy (FCCS) measurements to investigate simultaneous binding of both entities to single particles (Figure 4, lower right). In a solution containing equimolar amounts of both proteins the cross correlation showed high coincidence of H₆-GFP and H₆-Tf* after addition of Zr-fum NPs (solid gray), which demonstrated binding of different His-tagged proteins to the same Zr-fum particles. Importantly, both FCS and FCCS experiments revealed the colloidal stability of the MOF NPs. Additionally, the framework stability of the particles prior to and after functionalization under aqueous conditions was investigated by XRD measurements (Figures S3–S5). The experiments showed the nearly unchanged crystallinity of all samples under each tested condition. In the case of Zr-fum MOF NPs, this was also confirmed by SEM and DLS measurements, exhibiting no observable change in morphology of dried particles and moderate effect on hydrodynamic size of dispersed particles upon modification with H₆-Acr in HBG pH 7.4 (Figures S2 and S16).

Cellular Uptake of Model Peptides and Proteins with MOF NPs. To assess the potential of MOF NPs to mediate cellular internalization of biomacromolecules, H₆-carboxyfluorescein (H₆-CF), recombinant eGFP with genetically encoded His-tag (H₆-GFP) and chemically His-tagged and ATTO 647N labeled human transferrin (H₆-Tf*) were used as fluorescent model compounds. Based on the photometrical analysis of His-tag binding to the three MOF species (Figure 2d), the His-tagged functional units were used at a ratio of 10 nmol of H₆-tag per 1 mg of MOF which is considerably below the determined binding capacities of 192 nmol/mg MIL88A, 208 nmol/mg HKUST-1 and 24 nmol/mg Zr-fum. First, cell viability of HeLa cells after incubation with different amounts of all three MOF NPs and different His-tags for 48 h was evaluated by MTT-assay (Figure S20). MIL-88A, Zr-fum, and the tested His-tags H₆-CF, H₆-GFP, and H₆-Tf* were very well tolerated. HKUST-1 exhibited considerable cytotoxicity, which could be avoided by shortening the incubation time with cells to 2 h followed by medium exchange, which deleted observable effects on metabolic activity at the end point evaluation after 48 h (Figure S20b). Next, cellular uptake of the different MOF NPs after functionalization with the H₆-tagged fluorescent dye H₆-CF or H₆-GFP was investigated. For prefunctionalization by coordinative self-assembly, His-tags and MOF NPs were mixed at a final concentration of 10 μ M H₆-tag and 1 mg/mL MOF in HBG buffer (ratio of 10 nmol H₆-tag per 1 mg MOF) and incubated for 15 min at room temperature. Cells were then incubated with the different functionalized MOF NPs for 24 h in medium at a concentration of 0.1 mg/mL MOF corresponding to 1 μ M His-tag, followed by flow cytometry

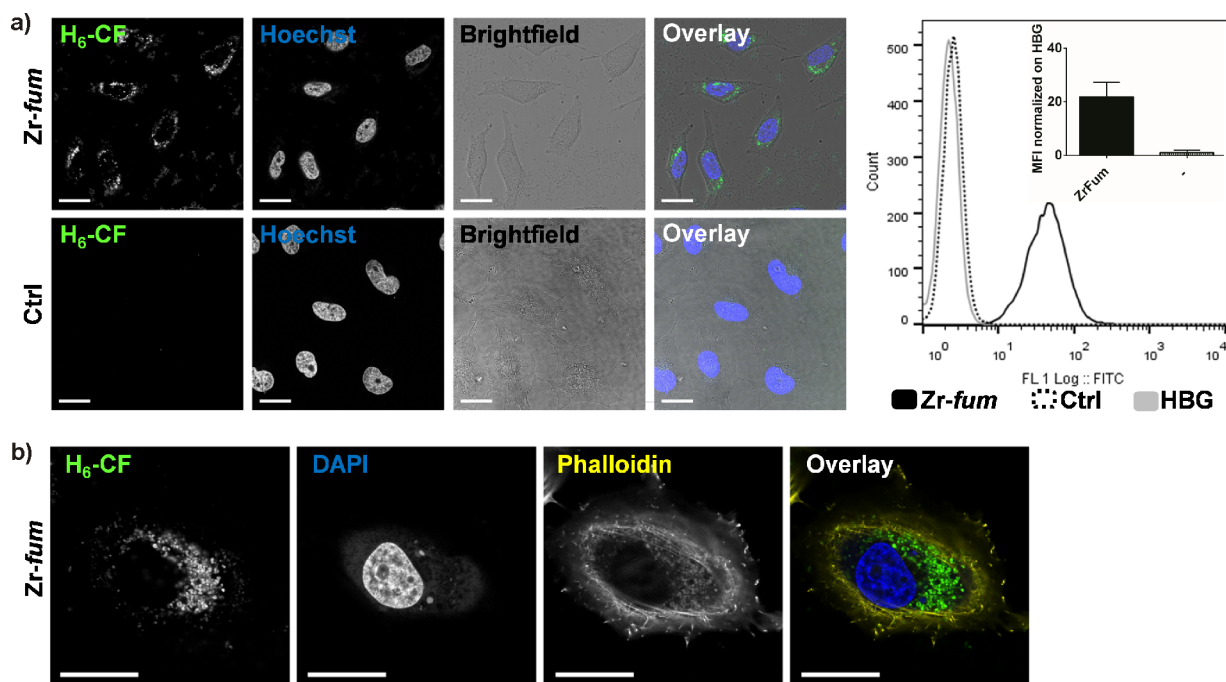


Figure 5. Cellular uptake of fluorescent peptide H_6 -CF mediated by *Zr-fum* NPs. H_6 -CF was incubated with *Zr-fum* MOF NPs for 15 min at room temperature in HBG for prefunctionalization by coordinative self-assembly. The functionalized particles were incubated with HeLa cells for 24 h at a concentration of 0.1 mg/mL *Zr-fum* corresponding to 1 μ M H_6 -CF. Solutions containing H_6 -CF at same concentration but no *Zr-fum* NPs served as control (Ctrl). (a) Confocal laser scanning microscopy (CLSM, left) and flow cytometry (right) after incubation of HeLa cells with functional NPs *Zr-fum*/ H_6 -CF (*Zr-fum*, CLSM upper row, flow cytometry solid black), H_6 -CF control without *Zr-fum* NPs (Ctrl, CLSM lower row, flow cytometry dotted black) or HBG (flow cytometry gray). Mean fluorescence intensity (MFI) was normalized to HBG and is depicted in the inset. CLSM left to right: green fluorescence of H_6 -CF, nuclear staining with Hoechst dye, brightfield image, overlay of all three channels. (b) Enlarged CLSM image of a fixed HeLa cell after incubation with *Zr-fum*/ H_6 -CF. Left to right: green fluorescence of H_6 -CF, nuclear staining with DAPI dye, actin staining with rhodamine-phalloidin, overlay of all three channels. Scale bar: 25 μ m. Additional images can be found in Supporting Information Figures S23 and S24.

and confocal laser scanning microscopy (CLSM) (Figures 5, S21, S22a, and S23–S26). MIL-88A and HKUST-1 MOF NPs showed low levels of detectable cellular uptake (Figure S21) presumably due to the presence of huge particles with a tendency to aggregate (Figures S1 and S10–S13) and fluorescence quenching effects (Figure S18). Compared to MIL-88A and HKUST-1, *Zr-fum* MOF NPs exhibit several favorable characteristics such as very narrow particle size distribution, uniform sphere morphology, low aggregation behavior, negligible fluorescence quenching and also good cellular tolerance. Thus, despite their comparatively low His-tag binding capacity, they were selected to be used for further experiments. *Zr-fum*/ H_6 -CF showed cellular uptake in CLSM (Figure 5a, left) and flow cytometry (Figure 5a, right). Additional z-stacks of CLSM images can be found in Figures S23 and S24. The mean fluorescence intensity (MFI, inset) of cells treated with *Zr-fum*/ H_6 -CF increased 20-fold compared to free H_6 -CF. The cellular uptake of *Zr-fum*/ H_6 -GFP alone is depicted in Figures S22a, S25, and S26 showing 30-fold higher MFI values compared to free H_6 -GFP. A 3D reconstruction movie of a cell treated with *Zr-fum*/ H_6 -GFP is provided in the Supporting Information.

A distinct advantage of the self-assembly concept demonstrated here is the possible one-step multifunctionalization of MOF NPs by simultaneously mixing of different H_6 -tagged functional units with bare MOF NPs (Figure 1c). This procedure facilitates the creation of multifunctional MOF NPs with various stoichiometric ratios as required for optimization of spatiotemporal co-delivery into cells. As the

simultaneous assembly of H_6 -GFP and H_6 -Tf* with *Zr-fum* MOF NPs had been confirmed by FCCS measurements (Figure 4, lower right), HeLa cells were subjected to these double-functionalized particles (*Zr-fum*/ H_6 -GFP + H_6 -Tf*) for 24 h at a concentration of 0.1 mg/mL MOF corresponding to 0.5 μ M H_6 -GFP and H_6 -Tf*, followed by investigation of the internalization (Figures 6 and S22b). Considerable colocalization of H_6 -GFP and H_6 -Tf* could be observed (Figure 6a, upper row and 6b). In contrast to free H_6 -GFP, free H_6 -Tf* was also taken up by the cells without the addition of *Zr-fum* MOF NPs to a certain extent (Figure 6a, lower row). This can be explained by the fact that HeLa cells express the transferrin receptor (Figure S29), thus enabling receptor-mediated uptake of free H_6 -Tf*. However, despite the MOF-independent uptake route of H_6 -Tf*, association with *Zr-fum* resulted in 5-fold higher internalization, confirming an additional boost due to NP mediated uptake. Additional z-stacks of CLSM images can be found in Figures S27 and S28. Looking at the intracellular distribution of fluorescent peptides and proteins internalized via *Zr-fum* MOF NPs in detail, the spotty arrangement indicates high vesicular entrapment and suggests endosomal escape being a hurdle for cytosolic delivery.

Endocytosis Mechanism. The cellular uptake pathway of *Zr-fum*/ H_6 -GFP NPs was investigated in an uptake experiment (Figure 7). HeLa cells were preincubated for 30 min at 4 $^{\circ}$ C, to reduce cellular metabolism and block energy dependent processes, or with various concentrations of the individual endocytosis inhibitors chlorpromazine (clathrin-mediated endocytosis), amiloride (macropinocytosis) and genistein

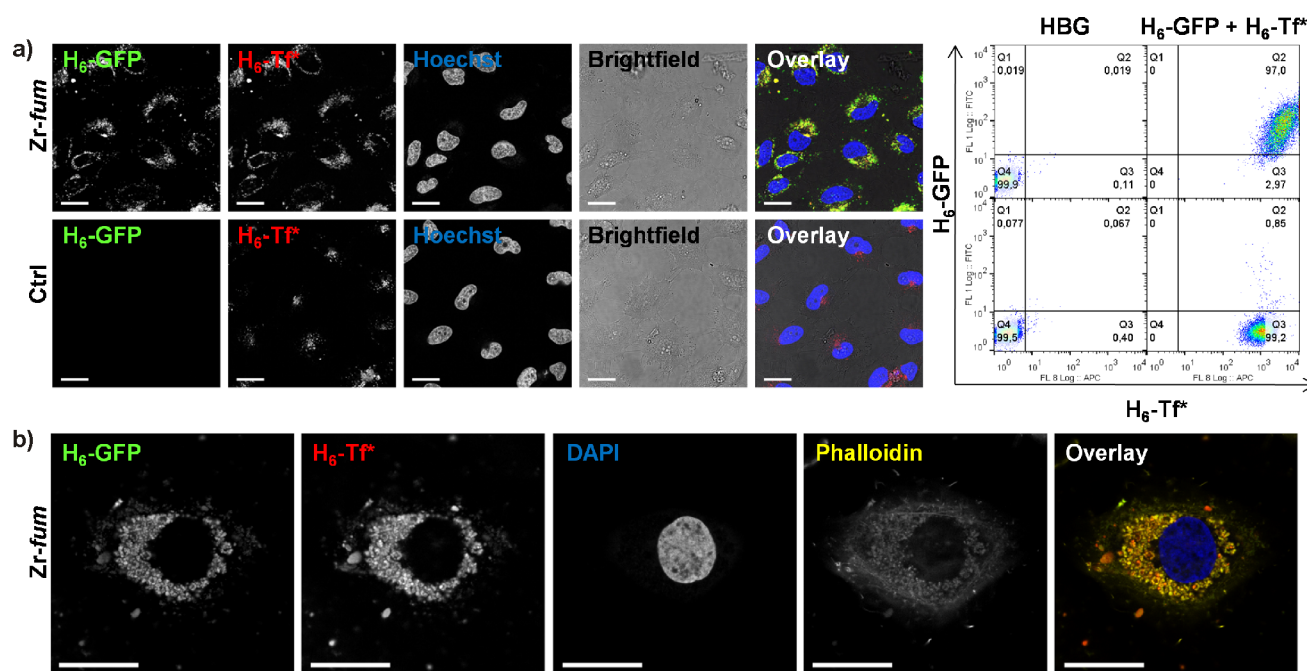


Figure 6. Simultaneous cellular uptake of fluorescent proteins H₆-GFP and H₆-Tf* mediated by Zr-fum NPs. An equimolar mixture of H₆-GFP and H₆-Tf* was incubated with Zr-fum MOF NPs for 15 min at room temperature in HBG for prefunctionalization by coordinative self-assembly. The double functionalized particles were incubated with HeLa cells for 24 h at a concentration of 0.1 mg/mL Zr-fum corresponding to 0.5 μM H₆-GFP and H₆-Tf*. Solutions containing H₆-GFP and H₆-Tf* at same concentration but no Zr-fum NPs served as control (Ctrl). (a) Cellular uptake of Zr-fum/H₆-GFP+H₆-Tf* (upper row) or control without MOF NPs (lower row). CLSM left to right: green fluorescence of H₆-GFP, red fluorescence of H₆-Tf*, nuclear staining with Hoechst dye, brightfield picture, overlay of all four channels, yellow color indicates colocalization of H₆-GFP and H₆-Tf*. Flow cytometry analysis: HBG (left) or H₆-GFP + H₆-Tf* (right) with Zr-fum MOF NPs (upper row) or Ctrl without MOF NPs (lower row). (b) Enlarged CLSM image of a fixated HeLa cell after incubation with Zr-fum/H₆-GFP + H₆-Tf*. Left to right: green fluorescence of H₆-GFP, red fluorescence of H₆-Tf*, nuclear staining with DAPI dye, actin staining with rhodamine-phalloidin, and overlay of all four channels. Scale bar: 25 μm. Additional images can be found in Figures S27 and S28, and a 3D reconstruction movie of a cell treated with Zr-fum/H₆-GFP is provided in the Supporting Information.

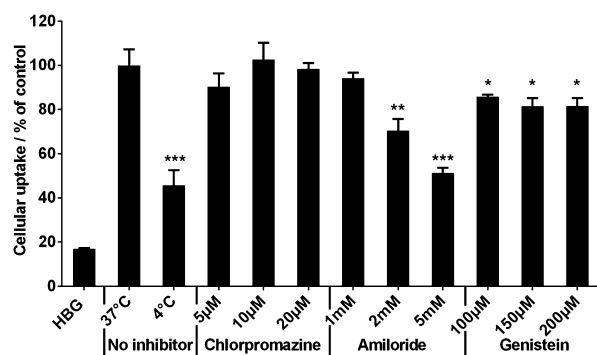


Figure 7. Evaluation of endocytosis inhibition of Zr-fum/H₆-GFP nanoparticles. Pre-Incubation of HeLa cells with different inhibitors or at 4 °C for 30 min, followed by incubation with Zr-fum/H₆-GFP for 2 h at 37 °C or 4 °C. Flow cytometric analysis was carried out in PBS (pH 4.0) to quench the extracellular fluorescence. Cellular uptake was determined as MFI. Data are presented as % cellular uptake normalized to uptake of Zr-fum/H₆-GFP NPs at 37 °C ± SD (n = 3).

(caveolae-mediated endocytosis) to discriminate the particular endocytotic routes. Afterward the cells were subjected to Zr-fum/H₆-GFP NPs at a concentration of 0.1 mg/mL MOF NPs corresponding to 1 μM H₆-GFP for 2 h, followed by flow cytometric analysis in acidified PBS (pH 4, 10% FBS) to quench the extracellular fluorescence. The results clearly show, that the NPs are internalized via an energy dependent process. Preincubation with amiloride showed the greatest inhibitory effect which suggests macropinocytosis is having major

contribution to the uptake of Zr-fum/H₆-GFP nanoparticles. Since some effect of genistein was observed, caveolae mediated uptake might also be involved to a minor extent. A recent study investigated the endocytosis mechanisms of UiO-66 (Zr⁴⁺/terephthalate) MOF NPs.⁶¹ Consistently, the cellular uptake of UiO-66 was also identified to be an energy dependent process with distinct involvement of macropinocytosis; however, also a major contribution of clathrin-mediated endocytosis was found.

Transduction of Biologically Active Peptides and Proteins. To further evaluate the potential of Zr-fum MOF NPs as carrier system for cytosolic cargo release, transduction of membrane impermeable bioactive pro-apoptotic peptides (Bak, Bad, KLK) and mitochondrial cytochrome c (CytC) protein was investigated and cell killing was used as reporter of successful cytosolic delivery. H₆-tags were used as reporter of successful cytosolic delivery. H₆-tags were chemically conjugated to CytC or integrated at the N-terminus of the peptide sequences derived from the BH3 domain of Bak and Bad proteins⁶² or the antibacterial and mitochondrial membrane-disruptive artificial peptide KLK.^{63,64} Endogenous cellular CytC represents an essential part of the electron transfer chain in mitochondria but also a crucial player in the intrinsic mitochondrial apoptosis pathway after release into the cytosol.⁶⁵ Several approaches for the intracellular delivery of exogenous CytC, induction of apoptosis and cell killing have been reported before.^{66–69} Notably, for the purification of H₆-CytC (and H₆-Tf*) carrying a H₆-tag after chemical conjugation, immobilized metal-ion chromatography was used, which is based on the same principle as the binding to

MOFs. The utilization of the same interaction for isolation and subsequent attachment to the carrier system is considered a very convenient and robust manufacturing process. Binding of the pro-apoptotic factors to *Zr-fum* NPs was confirmed by measuring the change of zeta potential upon addition of the MOFs (Figure S30a). For biological evaluation, HeLa cells were treated with *Zr-fum*/H₆-Bak, /H₆-Bad, /H₆-KLK, or /H₆-CytC (0.2 mg/mL *Zr-fum* and 10 μM peptide or protein) for 48 h. Cell viability was assessed by MTT assay and approximately 60% cell killing could be detected in case of all functionalized *Zr-fum* NPs (Figure 8).

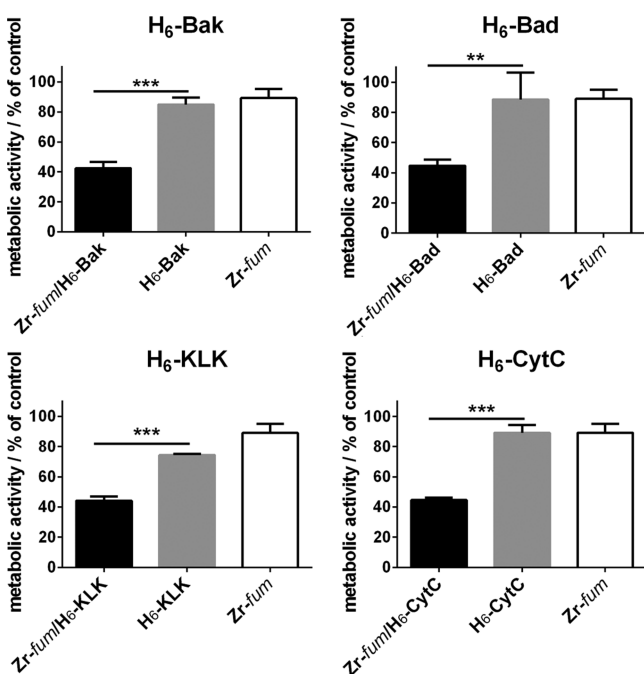


Figure 8. Intracellular transport of pro-apoptotic factors by *Zr-fum* MOF NPs and induction of HeLa cell killing upon incubation for 48 h. Final concentration of H₆-Bak, H₆-Bad, H₆-KLK, and H₆-CytC was 10 μM (0.2 mg *Zr-fum*/10 nmol His-tag per mL medium). Data are presented as percent of metabolic activity of control cells ± SD (*n* = 3) (MTT assay).

Without the addition of MOF NPs all pro-apoptotic factors did not exhibit any detectable toxicity up to a concentration of 20 μM (Figure S30b). These findings indicate that, despite the bottleneck of vesicular entrapment, significant fractions of cargo molecules were able to escape and induce biological effects in the cytosol.

CONCLUSION

In summary, the proposed coordinative interaction of functionalized His-tags with MOF NPs was successfully established, exhibiting His-tag length and MOF species dependent binding. The fact that all investigated MOF structures showed considerable H₆-tag binding, despite their different metal components, provided flexibility for consideration of additional parameters and material characteristics (e.g., particle size distribution, aggregation behavior, fluorescence quenching and cytotoxicity) relevant for the intended purpose. The inherent properties of the individual compounds (His-tag containing functional units, MOF NPs) and the reversible nature of interaction account for the strength of the approach. Numerous available recombinant proteins already contain His-

tags or they can readily be integrated in peptidic structures by conjugation. For biomedical applications, MOF NPs are promising materials due to their precise assembly of an enormous number of inorganic and organic molecular building blocks resulting in a highly variable chemical composition, porosity and degradability into their small building units. The MOF structural designability at the molecular level chemistry together with an extension of the functional unit library opens the perspective to generate a variety of “self-assembling multifunctional coordination particles” (SAMCOPs) by simple combinatorial and stoichiometric mixing. In this respect, this work presents a versatile functionalization concept of MOF NPs with great potential for co-delivery of proteins, drugs, or other pharmacologically active agents, including those that can be adsorbed within the pore systems.

METHODS

Synthesis of MIL-88A. MIL-88A was synthesized using an approach based on the results of Chalati et al.⁵² FeCl₃·6H₂O (1.084 g, 4.01 mmol) and fumaric acid (485 mg, 4.18 mmol) were given into water (20 mL). After FeCl₃·6H₂O was completely dissolved, the reaction vessel was placed in a microwave reactor (Synthos 3000, Anton Paar). In addition to the reaction vessel, a reference vessel containing an aqueous solution of FeCl₃·6H₂O (1.080 g, 20 mL) and two vessels containing water (20 mL) were placed in the microwave reactor. The sample was heated in 30 s to 80 °C, stayed at 80 °C for 5 min and cooled down to room temperature in 1 h.

Synthesis of HKUST-1. The synthesis of HKUST-1 was conducted following a method shown by Huo et al.⁴⁷ Cu(NO₃)₂·2.5H₂O (70 mg, 0.30 mmol) was dissolved in water (6 mL). Trimesic acid (126 mg, 0.60 mmol) was added to this solution under stirring. The reaction mixture was left stirring for 60 min. Subsequently, the resulting product was washed via centrifugation (15 min, 8750 rpm). The supernatant was removed and the precipitated nanoparticles were dispersed in ethanol (6 mL). This washing cycle was repeated three times to yield the final product.

Synthesis of *Zr-fum*. *Zr-fum* were synthesized using an approach based on the results of Wißmann et al.⁴⁸ ZrCl₄ (120.4 mg, 0.52 mmol) and fumaric acid (180.1 mg, 1.54 mmol) were given into a glass vessel (25 mL). A mixture of water (10 mL) and formic acid (975 μL) was added to the glass reactor. After sealing the reactor the dispersion was placed in an oven (120 °C) for 24 h. Subsequently, the reaction mixture was cooled down to room temperature followed by separation into eight equal portions. The nanoparticle dispersions were washed in a first step via centrifugation (4 min, 14 000 rpm) and subsequent redispersion in water (8 × 1.5 mL) under sonication. The samples were further washed in three additional washing cycles comprising centrifugation (4 min, 14 000 rpm), removal of the supernatant, and redispersion of the remaining nanoparticles in ethanol (8 × 1.5 mL). Afterward, the eight dispersions were reunified.

Preparation of MOF Suspension in HBG. MOF suspensions in HBG were always freshly prepared prior to performing the experiment. The necessary amount of MOF material in ethanol was centrifuged (10 min, 10 000 rpm), and the supernatant was removed. The MOF pellet was resuspended in HBG (pH 7.4) at a final concentration of 5 or 10 mg/mL by continuous pipetting, followed by 10 min sonication.

Investigation of Peptide Binding (A₆, H₆) by RP-HPLC. Three μL of a solution containing equimolar amounts of H₆-Acr and A₆-Acr (5 mM) in HBG (pH 7.4) were added to 47 μL HBG in a 1.5 mL reaction tube. 100 μL of MOF suspension (5 mg/mL in HBG, pH 7.4) were added and vortexed briefly. As control, 100 μL HBG without MOF particles were added to an analogous sample. The mixtures were incubated at room temperature for 15 min under shaking and centrifuged for 10 min at 13 400 rpm. Subsequently, the supernatant (120 μL) was transferred into HPLC sample vials. RP-HPLC analysis was carried out using a YMC Pack Pro C18 RS column (250 × 4.6 mm) connected to a VWR Hitachi Chromaster HPLC system (5160 pump module, 5260 auto sampler, 5310 column oven, 5430 diode

array detector). A volume of 10 μL of the samples was injected, and a gradient from 5% acetonitrile (0.1% TFA) to 100% acetonitrile (0.1% TFA) over 15 min was used for the analysis. Acridine containing compounds were detected photometrically at 360 nm.

Zeta Potential Measurements of MOF Nanoparticle Functionalization. $\text{H}_6\text{-Acr}$ or $\text{A}_6\text{-Acr}$ (3 nmol) was diluted in HBG (pH 7.4) buffer. In case of pro-apoptotic peptides and CytC, an amount of 5 nmol was used. Next, the amount of 100 μg of MOF NPs (5 mg/mL, HBG pH 7.4) was added (final volume 30 μL) and samples were incubated at room temperature for 15 min with shaking. Shortly before the measurement in a folded capillary cell (DTS1070), samples were diluted to a final MOF concentration of 0.1 mg/mL. Zeta potential was measured by electrophoretic laser-light scattering using a Zetasizer Nano ZS (Malvern Instruments, Worcestershire, U.K.). Zeta potentials were calculated by using the Smoluchowski equation, and each sample was measured three times with 10 to 30 subruns at 25 $^\circ\text{C}$.

Quantitative Determination of H_0 -, H_3 -, and H_6 -Acr Binding to MOF NPs. A solution containing a total amount of 130 nmol oligopeptide-based structure to be examined was prepared in HBG. The required amount of 10 mg/mL MOF nanoparticles dispersed in HBG was added featuring a total volume of 1 mL. Right after the addition of the MOF nanoparticles, samples were briefly vortexed. After subsequent incubation (15 min, 25 $^\circ\text{C}$, 600 rpm) and centrifugation (5 min, 14 000 rpm), the supernatant (100 μL) was collected and photometrically measured at 360 nm against HBG as a blank. For each examined oligopeptide-based structure, a control of 130 nmol peptide without MOF in a total volume of 1 mL was also prepared and measured ($n = 3$). To obtain the amount of bound peptide, the absorption of the supernatant, representing the amount of peptide that remained in solution and thereby unbound by the MOF, was subtracted from the average absorption of the MOF free control: $A(\text{bound}) = A(\text{control}) - A(\text{supernatant})$. Final binding values were calculated as follows, $\%(\text{bound}) = A(\text{bound})/A(\text{control}) \times 100$. The average of percent bound determined in three independent measurements \pm SD was plotted.

Investigation of Binding Stability of H_6 -tags to Zr-*fum* and pH Dependent Release. In order to evaluate the stable binding and extent of acidic release of His-tags and Zr-*fum* MOF NPs over a longer period, Zr-*fum* NPs in HBG were loaded with $\text{H}_6\text{-A647N}$. 50 μL of the freshly prepared Zr-*fum* NPs were diluted in \sim 500 μL of HBG pH 7.4 (depending on the amount of HCl added to the sample in the next step), followed by addition of 4 μL of 1 mM $\text{H}_6\text{-A647N}$. The HBG volume therefore slightly varied in order to always allow for equal final sample volumes of 500 μL . Samples were briefly vortexed and incubated under agitation for 15 min (25 $^\circ\text{C}$, 600 rpm, light protection). Afterward, samples were acidified to pH 3, pH 5, and pH 7.4 by addition of 9.2, 4.5, or 0 μL of 1 M HCl, respectively. After 0.5, 3, and 24 h, the respective samples were centrifuged (5 min, 14 000 rpm). The presence of free dye in the supernatant was determined photometrically at 646 nm ($n = 3$). Independent samples were used for each time point.

Fluorescence Correlation Spectroscopy (FCS). The non-fluorescent MOF nanoparticles are not detectable by the FCS unless fluorescently labeled His-tags are attached to the NPs. Thus, a shift to higher diffusion times of the correlation curve after addition of NPs to fluorescently labeled His-tags certifies the binding of His-tags to the NPs surface. Normalization of autocorrelation curves helps to clearly visualize that the autocorrelation function of the MOF/His-tag is shifted toward higher correlation times with respect to the free His-tag molecules. Dual-color fluorescence cross-correlation spectroscopy (FCCS) allows for a comparison between spectrally separated channels to extract codiffusion events that reflect interactions between differently labeled molecules.^{70,71} For FCS and FCCS measurements, an Axiovert 200 microscope with a ConfoCor 2 unit (Carl Zeiss, Jena, Germany) equipped with a 40 \times (NA 1.2) water immersion apochromat objective (Carl Zeiss) was used. A helium neon laser (633 nm) and for FCCS additionally an argon laser (488 nm) was used for illumination. Samples were measured in eight-well LabTek chamber slides (Nunc, Rochester, NY). If nothing else mentioned, measurements were performed in HBG pH 7.4 at a

temperature of 22.5 $^\circ\text{C}$. Correlation was performed using ConfoCor 2 software. A detailed description of the various experimental setups of FCS and FCCS measurements and the theory of FCS can be found in the Supporting Information.

Cell Culture. HeLa cells were grown in Dulbecco's Modified Eagle's Medium (DMEM) (1000 mg/mL glucose, L-glutamine and sodium bicarbonate) supplemented with 10% FBS, 100 U/mL penicillin, 100 μg /mL streptomycin at 37 $^\circ\text{C}$ and 5% CO_2 in a humidified incubator.

Cellular Uptake Experiments Using Flow Cytometric Analysis. Cells were seeded in 24-well plates (Corning Costar, Sigma-Aldrich, Germany) at a density of 20 000 cells/well. After 24 h, medium was replaced with 400 μL of fresh medium. $\text{H}_6\text{-CF}$ or $\text{H}_6\text{-GFP}$ (0.5 nmol) was diluted in HBG (pH 7.4), 50 μg of MOF NPs (5 mg/mL in HBG, pH 7.4) were added (final volume 50 μL), and the solution was strongly mixed. For the co-delivery of $\text{H}_6\text{-GFP}$ and $\text{H}_6\text{-Tf}^*$, 0.25 nmol of $\text{H}_6\text{-GFP}$ and 0.25 nmol of $\text{H}_6\text{-Tf}^*$ were premixed in HBG (pH 7.4) before the amount of 50 μg of Zr-*fum* MOF NPs (5 mg/mL in HBG, pH 7.4) was added (final volume 50 μL). The mixtures were incubated for 15 min at room temperature, diluted 1:2 with HBG (pH 7.4, final volume 100 μL), and added to the cells (100 μL MOF/His-tag solution per well). Controls were performed without the addition of MOF NPs. Cells were incubated for 24 h at 37 $^\circ\text{C}$ and 5% CO_2 in a humidified incubator. In the case of HKUST-1 MOF NPs, medium was changed after 2 h and cells were incubated for further 22 h in fresh medium. Cells were washed with PBS (pH 7.4), detached with trypsin/EDTA and diluted with fresh medium. Cells were centrifuged and resuspended in 500 μL PBS containing 10% FBS at pH 4 to quench extracellular fluorescence. DAPI (4',6-diamidino-2-phenylindole) was added to a final concentration of 1 ng/ μL shortly before the measurement. The cellular fluorescence was assayed by excitation of DAPI at 405 nm and detection of emission at 450 nm, fluorescein at 488 nm and detection of emission at 510 nm. For the co-delivery of $\text{H}_6\text{-GFP}$ and $\text{H}_6\text{-Tf}^*$, the cellular fluorescence was also assayed by excitation of A647N at 635 nm and detection of emission at 665 nm. Cells were appropriately gated by forward/sideward scatter and pulse width for exclusion of doublets. DAPI was used to discriminate between viable and dead cells. Data were recorded by Cyan ADP flow cytometer (Dako, Hamburg, Germany) using Summit acquisition software (Summit, Jamesville, NY). Ten thousand gated cells per sample were collected. Analysis was done by FlowJo 7.6.5 flow cytometric analysis software. All experiments were performed in triplicate. MFI was calculated by FlowJo 7.6.5 flow cytometric analysis software and is depicted as normalization to HBG \pm SD ($n = 3$).

Confocal Laser Scanning Microscopy. Cells were seeded in 8-well Nunc chamber slights (Thermo Scientific, Germany) at a density of 12 000 cells/well. Wells were coated with collagen A prior to seeding. After 24 h, medium was replaced with 240 μL of fresh medium. The various samples were prepared in the same way as has been described above but in a final volume of 60 μL of HBG. MOF NPs (30 μg) were functionalized with 0.3 nmol of $\text{H}_6\text{-CF}$ or $\text{H}_6\text{-GFP}$ in 30 μL of HBG (pH 7.4). In the case of the co-delivery experiment, the amount of 0.15 nmol of $\text{H}_6\text{-GFP}$ was mixed with 0.15 nmol of $\text{H}_6\text{-Tf}^*$ before the addition of 30 μg of Zr-*fum* MOF NPs. After incubation of the mixtures for 15 min at room temperature, they were diluted 1:2 in HBG (pH 7.4, final volume 60 μL). The mixtures were added to the cells (60 μL MOF/His-tag solution per well) and incubated for 24 h. Controls were performed without the addition of MOF NPs. In the case of HKUST-1 MOF NPs, the medium was changed after 2 h and cells were incubated for further 22 h in fresh medium. Prior to imaging, nuclei were stained with Hoechst dye (1 ng/ μL). Medium was replaced by DMEM without phenol red supplemented with 10% FBS, 100 U/mL penicillin, and 100 μg /mL streptomycin, and cells were imaged using a Leica TCS SP8 confocal microscope with an 63 \times DIC oil immersion objective (Plan-APOCHROMAT). For imaging of z-stacks, cells were fixated for 30 min, using 4% (w/v) paraformaldehyde solution followed by three washes with PBS (pH 7.4). The nucleus was stained with DAPI (1 ng/ μL) and actin with rhoadmine-phalloidin (2 μL /mL) for 15 min at room temperature. Staining solution was replaced with PBS (pH 7.4),

and cells were stored at 4 °C. Images were recorded with a z-distance of 0.3 μm from basolateral (top) to apical (bottom) pole of a representative cell. Pictures were taken at 405 nm (Hoechst dye or DAPI), 488 nm ($\text{H}_6\text{-GFP}$ or $\text{H}_6\text{-CF}$), 514 nm (rhodamine-phalloidine), and 633 nm (ATTO 647N).

Endocytosis Inhibitory Assay. HeLa cells were seeded in 24-well plates (Corning Costar, Sigma-Aldrich, Germany) at a density of 50 000 cells/well. After 24 h, medium was replaced with 400 μL fresh medium containing the different endocytosis inhibitors, chlorpromazine (final concentration 5, 10, and 20 μM), amiloride (final concentration 1, 2, and 5 mM), and genistein (final concentration 100, 150, and 200 μM). Cells were preincubated with the different inhibitors or at 4 °C for 30 min before addition of the $\text{H}_6\text{-GFP/Zr-fum}$ MOF NPs. 0.5 nmol $\text{H}_6\text{-GFP}$ were diluted in HBG (pH 7.4), 50 μg Zr-fum MOF NPs (5 mg/mL in HBG, pH 7.4) were added (final volume 50 μL) and the solution was strongly mixed. The mixture was incubated for 15 min at room temperature, diluted 1:2 with HBG (pH 7.4, final volume 100 μL) and added to the cells (100 μL $\text{Zr-fum/H}_6\text{-GFP}$ solution per well). Cells were incubated for 2 h at 37 °C and 5% CO_2 or at 4 °C. Cells were washed with PBS (pH 7.4), detached with trypsin/EDTA, and diluted with fresh medium. Cells were centrifuged and resuspended in 500 μL of PBS containing 10% FBS at pH 4 to quench extracellular fluorescence. DAPI (1 ng/ μL) was added shortly before the measurement. The cellular fluorescence was assayed by excitation of DAPI at 405 nm and detection of emission at 450 nm, and fluorescein at 488 nm and detection of emission at 510 nm. Cells were appropriately gated by forward/sideward scatter and pulse width for exclusion of doublets. DAPI was used to discriminate between viable and dead cells. Data were recorded by Cyan ADP flow cytometer (Dako, Hamburg, Germany) using Summit acquisition software (Summit, Jamesville, NY). Five thousand gated cells per sample were collected. Analysis was done by using FlowJo 7.6.5 flow cytometric analysis software. Data is presented as percentage of cellular uptake of $\text{Zr-fum/H}_6\text{-GFP}$ NPs at 37 °C \pm SD ($n = 3$).

Delivery of Pro-apoptotic Peptides and CytC. Cells were seeded in 96-Well plates (Corning Costar, Sigma-Aldrich, Germany) at a density of 4000 cells/well. After 24 h, medium was replaced with 80 μL fresh medium. Then 1 nmol of $\text{H}_6\text{-Bak}$, $\text{H}_6\text{-Bad}$, $\text{H}_6\text{-Klk}$, or $\text{H}_6\text{-CytC}$ was diluted in HBG (pH 7.4), and the amount of 20 μg of Zr-fum MOF NPs (5 mg/mL in HBG pH 7.4) was added followed by strongly mixing of the samples (final volume 10 μL). Controls were performed without the addition of Zr-fum MOF NPs. The mixtures were incubated for 15 min at room temperature, diluted 1:2 with HBG (pH 7.4, final volume 20 μL), added to the cells (20 μL Zr-fum/His-tag solution per well), and incubated for 48 h. Analysis of cytotoxicity was carried out by MTT assay, as is described in the following.

Cell Viability Assay. Cells were seeded in 96-well plates (Corning Costar, Sigma-Aldrich, Germany) at a density of 4000 cells/well. After 24 h, medium was replaced with 80 μL of fresh medium. The appropriate amount of compound to be tested was diluted in HBG (pH 7.4), and a sample volume of 20 μL was added per well. Cells were incubated for 48 h at 37 °C and 5% CO_2 in a humidified incubator. Then a solution of MTT (3-(4,5-dimethylthiazol-2-yl)-2,5-diphenyltetrazolium bromide) (10 μL , 5 mg/mL) was added to each well, reaching a final concentration of 0.5 mg/mL. After an incubation time of 2 h, unreacted dye and medium were removed and the 96-well plates were frozen at -80 °C for at least 30 min. To dissolve the purple formazan product, DMSO (100 μL /well) was added and the plate was incubated for 30 min at 37 °C with shaking. The wells were quantified by measuring absorbance at 590 nm with background correction at 630 nm using a microplate reader (TecanSpectrafluor Plus, Tecan, Switzerland). All studies were performed in triplicate. The relative cell viability (%) related to control wells treated only with 20 μL of HBG (pH 7.4) was calculated as $([A] \text{ test}/[A] \text{ control}) \times 100\%$.

Statistical Analysis. The statistical significance of experiments was analyzed using the *t* test; **** $p \leq 0.0001$, *** $p \leq 0.001$, ** $p \leq 0.01$, and * $p \leq 0.05$.

■ ASSOCIATED CONTENT

§ Supporting Information

The Supporting Information is available free of charge on the ACS Publications website at DOI: 10.1021/jacs.6b11934.

Additional materials and methods, synthesis and analysis of peptides and His-tagged functional units, characterization of MOF NPs (PDF)

Movie demonstrating the binding of $\text{H}_6\text{-A647N}$ to HKUST-1 MOF NPs visualized by decoloration of the supernatant after centrifugation (AVI)

Three-dimensional reconstruction movie of a HeLa cell treated with $\text{Zr-fum/H}_6\text{-GFP}$ (AVI)

■ AUTHOR INFORMATION

Corresponding Authors

*ulrich.laechelt@cup.uni-muenchen.de

*stefan.wuttke@cup.lmu.de

ORCID

Ernst Wagner: 0000-0001-8413-0934

Ulrich Lächelt: 0000-0002-4996-7592

Notes

The authors declare no competing financial interest.

■ ACKNOWLEDGMENTS

We are grateful for financial support from the Excellence Cluster Nanosystems Initiative Munich (NIM) and the Center for NanoScience Munich (CeNS). Funding through the DFG SFB 1032 and DFG project WU 622/4-1 is greatly appreciated. We thank Olga Brück and Wolfgang Rödl for technical assistance and appreciate the help of cameraman Michael Beetz.

■ REFERENCES

- (1) Goesmann, H.; Feldmann, C. *Angew. Chem., Int. Ed.* **2010**, *49*, 1362.
- (2) Tibbitt, M. W.; Dahlman, J. E.; Langer, R. *J. Am. Chem. Soc.* **2016**, *138*, 704.
- (3) Calandra, P.; Caschera, D.; Turco Liveri, V.; Lombardo, D. *Colloids Surf., A* **2015**, *484*, 164.
- (4) Torchilin, V. P. *Pharm. Res.* **2007**, *24*, 1.
- (5) Nishiyama, N.; Matsumura, Y.; Kataoka, K. *Cancer Sci.* **2016**, *107*, 867.
- (6) Discher, B. M.; Won, Y. Y.; Ege, D. S.; Lee, J. C.; Bates, F. S.; Discher, D. E.; Hammer, D. A. *Science* **1999**, *284*, 1143.
- (7) Davis, M. E. *Mol. Pharmaceutics* **2009**, *6*, 659.
- (8) Park, I. K.; von Recum, H. A.; Jiang, S.; Pun, S. H. *Langmuir* **2006**, *22*, 8478.
- (9) Sanvicens, N.; Marco, M. P. *Trends Biotechnol.* **2008**, *26*, 425.
- (10) Jia, F.; Liu, X.; Li, L.; Mallapragada, S.; Narasimhan, B.; Wang, Q. *J. Controlled Release* **2013**, *172*, 1020.
- (11) Torchilin, V. P. *Annu. Rev. Biomed. Eng.* **2006**, *8*, 343.
- (12) Fu, A.; Tang, R.; Hardie, J.; Farkas, M. E.; Rotello, V. M. *Bioconjugate Chem.* **2014**, *25*, 1602.
- (13) Furukawa, H.; Cordova, K. E.; O'Keeffe, M.; Yaghi, O. M. *Science* **2013**, *341*, 1230444.
- (14) Zhou, H. C.; Long, J. R.; Yaghi, O. M. *Chem. Rev.* **2012**, *112*, 673.
- (15) Zhou, H. C.; Kitagawa, S. *Chem. Soc. Rev.* **2014**, *43*, 5415.
- (16) Horcajada, P.; Chalati, T.; Serre, C.; Gillet, B.; Sebrie, C.; Baati, T.; Eubank, J. F.; Heurtaux, D.; Clayette, P.; Kreuz, C.; Chang, J. S.; Hwang, Y. K.; Marsaud, V.; Bories, P. N.; Cynober, L.; Gil, S.; Ferey, G.; Couvreur, P.; Gref, R. *Nat. Mater.* **2010**, *9*, 172.
- (17) Baati, T.; Horcajada, P.; Gref, R.; Couvreur, P.; Serre, C. *J. Pharm. Biomed. Anal.* **2011**, *56*, 758.

- (18) Wuttke, S.; Zimpel, A.; Bein, T.; Braig, S.; Stoiber, K.; Vollmar, A.; Muller, D.; Haastert-Talini, K.; Schaeske, J.; Stiesch, M.; Zahn, G.; Mohmeyer, A.; Behrens, P.; Eickelberg, O.; Bolukbas, D. A.; Meiners, S. *Adv. Healthcare Mater.* **2017**, *6*, 1600818.
- (19) Taylor-Pashow, K. M.; Della Rocca, J.; Xie, Z.; Tran, S.; Lin, W. *J. Am. Chem. Soc.* **2009**, *131*, 14261.
- (20) Zheng, H.; Zhang, Y.; Liu, L.; Wan, W.; Guo, P.; Nystrom, A. M.; Zou, X. *J. Am. Chem. Soc.* **2016**, *138*, 962.
- (21) Yang, Y.; Hu, Q.; Zhang, Q.; Jiang, K.; Lin, W.; Yang, Y.; Cui, Y.; Qian, G. *Mol. Pharmaceutics* **2016**, *13*, 2782.
- (22) Wuttke, S.; Braig, S.; Preiss, T.; Zimpel, A.; Sicklinger, J.; Bellomo, C.; Radler, J. O.; Vollmar, A. M.; Bein, T. *Chem. Commun. (Cambridge, U. K.)* **2015**, *51*, 15752.
- (23) He, C.; Lu, K.; Liu, D.; Lin, W. *J. Am. Chem. Soc.* **2014**, *136*, 5181.
- (24) Tan, L.-L.; Li, H.; Qiu, Y.-C.; Chen, D.-X.; Wang, X.; Pan, R.-Y.; Wang, Y.; Zhang, S. X.-A.; Wang, B.; Yang, Y.-W. *Chem. Sci.* **2015**, *6*, 1640.
- (25) Wang, X. G.; Dong, Z. Y.; Cheng, H.; Wan, S. S.; Chen, W. H.; Zou, M. Z.; Huo, J. W.; Deng, H. X.; Zhang, X. Z. *Nanoscale* **2015**, *7*, 16061.
- (26) Levine, D. J.; Runcevski, T.; Kapelewski, M. T.; Keitz, B. K.; Oktawiec, J.; Reed, D. A.; Mason, J. A.; Jiang, H. Z.; Colwell, K. A.; Legendre, C. M.; FitzGerald, S. A.; Long, J. R. *J. Am. Chem. Soc.* **2016**, *138*, 10143.
- (27) Zhuang, J.; Kuo, C. H.; Chou, L. Y.; Liu, D. Y.; Weerapana, E.; Tsung, C. K. *ACS Nano* **2014**, *8*, 2812.
- (28) Wuttke, S.; Lismont, M.; Escudero, A.; Rungtaweivoranit, B.; Parak, W. J. *Biomaterials* **2017**, DOI: 10.1016/j.biomaterials.2017.01.025.
- (29) Liang, K.; Ricco, R.; Doherty, C. M.; Styles, M. J.; Bell, S.; Kirby, N.; Mudie, S.; Haylock, D.; Hill, A. J.; Doonan, C. J.; Falcaro, P. *Nat. Commun.* **2015**, *6*, 7240.
- (30) Liang, K.; Coghlan, C. J.; Bell, S. G.; Doonan, C.; Falcaro, P. *Chem. Commun. (Cambridge, U. K.)* **2016**, *52*, 473.
- (31) Lu, K.; He, C.; Lin, W. *J. Am. Chem. Soc.* **2015**, *137*, 7600.
- (32) Park, J.; Feng, D.; Yuan, S.; Zhou, H. C. *Angew. Chem., Int. Ed.* **2015**, *54*, 430.
- (33) Liu, J.; Yang, Y.; Zhu, W.; Yi, X.; Dong, Z.; Xu, X.; Chen, M.; Yang, K.; Lu, G.; Jiang, L.; Liu, Z. *Biomaterials* **2016**, *97*, 1.
- (34) Lismont, M.; Dreesen, L.; Wuttke, S. *Adv. Funct. Mater.* **2017**, DOI: 10.1002/adfm.201606314.
- (35) Horcajada, P.; Gref, R.; Baati, T.; Allan, P. K.; Maurin, G.; Couvreur, P.; Ferey, G.; Morris, R. E.; Serre, C. *Chem. Rev.* **2012**, *112*, 1232.
- (36) Rungtaweivoranit, B.; Zhao, Y.; Min Choi, K.; Yaghi, O. M. *Nano Res.* **2016**, *9*, 47.
- (37) Furukawa, S.; Reboul, J.; Diring, S.; Sumida, K.; Kitagawa, S. *Chem. Soc. Rev.* **2014**, *43*, 5700.
- (38) He, C.; Liu, D.; Lin, W. *Chem. Rev.* **2015**, *115*, 11079.
- (39) Zimpel, A.; Preiß, T.; Röder, R.; Engelke, H.; Ingrisich, M.; Peller, M.; Rädler, J. O.; Wagner, E.; Bein, T.; Lächelt, U.; Wuttke, S. *Chem. Mater.* **2016**, *28*, 3318.
- (40) McGuire, C. V.; Forgan, R. S. *Chem. Commun.* **2015**, *51*, 5199.
- (41) Block, H.; Maertens, B.; Priestersbach, A.; Brinker, N.; Kubicek, J.; Fabis, R.; Labahn, J.; Schafer, F. *Methods Enzymol.* **2009**, *463*, 439.
- (42) Hochuli, E.; Bannwarth, W.; Döbeli, H.; Gentz, R.; Stuber, D. *Bio/Technology* **1988**, *6*, 1321.
- (43) June, R. K.; Gogoi, K.; Eguchi, A.; Cui, X. S.; Dowdy, S. F. *J. Am. Chem. Soc.* **2010**, *132*, 10680.
- (44) Wieneke, R.; Latoria, N.; Rajan, M.; Kollmannsperger, A.; Natale, F.; Cardoso, M. C.; Tampe, R. *J. Am. Chem. Soc.* **2014**, *136*, 13975.
- (45) Postupalenko, V.; Desplancq, D.; Orlov, I.; Arntz, Y.; Spehner, D.; Mely, Y.; Klaholz, B. P.; Schultz, P.; Weiss, E.; Zuber, G. *Angew. Chem., Int. Ed.* **2015**, *54*, 10583.
- (46) Chiu, H. Y.; Deng, W.; Engelke, H.; Helma, J.; Leonhardt, H.; Bein, T. *Sci. Rep.* **2016**, *6*, 25019.
- (47) Huo, J.; Brightwell, M.; El Hankari, S.; Garai, A.; Bradshaw, D. J. *Mater. Chem. A* **2013**, *1*, 15220.
- (48) Wißmann, G.; Schaate, A.; Lilienthal, S.; Bremer, I.; Schneider, A. M.; Behrens, P. *Microporous Mesoporous Mater.* **2012**, *152*, 64.
- (49) Zahn, G.; Schulze, H. A.; Lippke, J.; König, S.; Sazama, U.; Fröba, M.; Behrens, P. *Microporous Mesoporous Mater.* **2015**, *203*, 186.
- (50) Ueda, E. K.; Gout, P. W.; Morganti, L. *Journal of chromatography. A* **2003**, *988*, 1.
- (51) Gaberc-Porekar, V.; Menart, V. *J. Biochem. Biophys. Methods* **2001**, *49*, 335.
- (52) Chalati, T.; Horcajada, P.; Gref, R.; Couvreur, P.; Serre, C. *J. Mater. Chem.* **2011**, *21*, 2220.
- (53) Baati, T.; Njim, L.; Neffati, F.; Kerkeni, A.; Bouttemi, M.; Gref, R.; Najjar, M.; Zakhama, A.; Couvreur, P.; Serre, C.; Horcajada, P. *Chem. Sci.* **2013**, *4*, 1597.
- (54) Lin, K.-Y. A.; Chang, H.-A.; Hsu, C.-J. *RSC Adv.* **2015**, *5*, 32520.
- (55) McKinlay, A. C.; Eubank, J. F.; Wuttke, S.; Xiao, B.; Wheatley, P. S.; Bazin, P.; Lavalley, J.-C.; Daturi, M.; Vimont, A.; De Weireld, G.; Horcajada, P.; Serre, C.; Morris, R. E. *Chem. Mater.* **2013**, *25*, 1592.
- (56) Hirschle, P.; Preiß, A.; Auras, F.; Pick, A.; Volkner, J.; Valdeperez, D.; Witte, G.; Parak, W. J.; Radler, J. O.; Wuttke, S. *CrystEngComm* **2016**, *18*, 4359.
- (57) Tay, C. Y.; Setyawati, M. I.; Xie, J.; Parak, W. J.; Leong, D. T. *Adv. Funct. Mater.* **2014**, *24*, 5936.
- (58) Martin, R.; Edsall, J. J. *J. Am. Chem. Soc.* **1960**, *82*, 1107.
- (59) Dietl, C.; Hintz, H.; Ruhle, B.; Schmedt Auf der Gunne, J.; Langhals, H.; Wuttke, S. *Chem. - Eur. J.* **2015**, *21*, 10714.
- (60) Wuttke, S.; Dietl, C.; Hinterholzinger, F. M.; Hintz, H.; Langhals, H.; Bein, T. *Chem. Commun. (Cambridge, U. K.)* **2014**, *50*, 3599.
- (61) Orellana-Tavra, C.; Mercado, S. A.; Fairen-Jimenez, D. *Adv. Healthcare Mater.* **2016**, *5*, 2261.
- (62) Li, R.; Boehm, A. L.; Miranda, M. B.; Shangary, S.; Grandis, J. R.; Johnson, D. E. *Neoplasia* **2007**, *9*, 801.
- (63) Javadpour, M. M.; Juban, M. M.; Lo, W. C.; Bishop, S. M.; Alberty, J. B.; Cowell, S. M.; Becker, C. L.; McLaughlin, M. L. *J. Med. Chem.* **1996**, *39*, 3107.
- (64) Ellerby, H. M.; Arap, W.; Ellerby, L. M.; Kain, R.; Andrusiak, R.; Rio, G. D.; Krajewski, S.; Lombardo, C. R.; Rao, R.; Ruoslahti, E.; Bredesen, D. E.; Pasqualini, R. *Nat. Med.* **1999**, *5*, 1032.
- (65) Bratton, S. B.; Salvesen, G. S. *J. Cell Sci.* **2010**, *123*, 3209.
- (66) Kim, S. K.; Foote, M. B.; Huang, L. *Biomaterials* **2012**, *33*, 3959.
- (67) Zhang, J.; Wu, L.; Meng, F.; Wang, Z.; Deng, C.; Liu, H.; Zhong, Z. *Langmuir* **2012**, *28*, 2056.
- (68) Ng, D. Y.; Fahrer, J.; Wu, Y.; Eisele, K.; Kuan, S. L.; Barth, H.; Weil, T. *Adv. Healthcare Mater.* **2013**, *2*, 1620.
- (69) Mendez, J.; Morales Cruz, M.; Delgado, Y.; Figueroa, C. M.; Orellano, E. A.; Morales, M.; Monteagudo, A.; Griebenow, K. *Mol. Pharmaceutics* **2014**, *11*, 102.
- (70) Schwille, P.; Meyer-Almes, F. J.; Rigler, R. *Biophys. J.* **1997**, *72*, 1878.
- (71) Rigler, R.; Földes-Papp, Z.; Meyer-Almes, F. J.; Sammet, C.; Volcker, M.; Schnetz, A. *J. Biotechnol.* **1998**, *63*, 97.